Current Applied Physics 10 (2010) 1169–1173

Contents lists available at ScienceDirect

Current Applied Physics

journal homepage: www.elsevier.com/locate/cap

Single cell-gap transflective liquid crystal device utilizing continuous director rotation with different twist angle in the fringe-field switching mode

Young Jin Lim [a], Jin Ho Kim [a], Jung Hwa Her [a], Myong-Hoon Lee [a], Wan-Seok Kang [b], Gi-Dong Lee [b,*], Seung Hee Lee [a,*]

[a] Department of Polymer. Nano Science and Technology, Chonbuk National University, Chonju, Chonbuk 561-756, Republic of Korea
[b] Department of Electronics Engineering, Dong-A University, Pusan 607-735, Republic of Korea

ARTICLE INFO

Article history:
Received 3 August 2009
Received in revised form 1 February 2010
Accepted 4 February 2010
Available online 12 February 2010

Keywords:
Transflective liquid crystal display
Fringe-field switching
Twist angle

ABSTRACT

In this paper, a single cell-gap and single gamma transflective liquid crystal displays (LCDs) associated with fringe-field switching (FFS) device is proposed. The device utilizes unique characteristic of the FFS device in which the twist angle of LC director is dependent on electrode position in on state. With optimization of pixel electrode width and distance between them, the LC director can be rotated about 22.5° and 45° of twist angles depending on electrode positions. Consequently, the parts with low and high twist angle could be played for the reflective (*R*) and transmissive (*T*) regions respectively, realizing a high image quality transflective display.

1. Introduction

Recently, as the application range of portable displays becomes broad, transflective liquid crystal displays (LCDs) with superior performance in any light environments such as sunlight or dark room are highly required. Various types of the transflective LCDs using different LC devices such as electrically controlled birefringence (ECB) [1], vertical alignment [2,3], in-plane switching [4,5], fringe-field switching (FFS) [6–8] have been proposed and some of them are commercialized. Among them, homogeneously aligned LC cells driven by fringe electric field (named as FFS device) have been extensively studied owing to its wide viewing angle and high transmittance (T/T_o) characteristics because the LC director mainly rotates in-plane above whole electrode surface [9–13]. One of the reported transflective FFS-LCDs has an in-cell retarder (ICR) with phase retardation of $\lambda/2$ on reflective (*R*) region [9]. This device has a less wavelength dependency in a dark state due to wide-band quarter-wave plate on the *R*-region but it has disadvantage of unmatched electro-optic characteristics on the *R*- and transmissive (*T*)-region due to dual cell-gap. Another type of transflective displays [11,12] use the FFS device in the *T*-region for wide viewing angle characteristics and the ECB device in the *R*-region; however, it has a disadvantage of additional process of patterning a common electrode on top substrate and did not show matched electro-optic characteristics. Some other types of transflective FFS-LCD proposed by our group [8,10,13] utilizing the concept of different twist angles in the *R*-region (22.5°) and at *T*-region (45°) in one pixel, however it also shows unmatched electro-optic curves due to different twist angles in the *R*- and *T*-regions. Hence, in order to match electro-optic characteristics for single gamma curves, fine patterns or different slit angles in the *R*- and *T*-regions are required so that the electro-optic curves in *R*- and *T*-regions in all grey scales can be perfectly matched.

In this paper, a transflective FFS-LCD using original characteristics of the FFS device, in which a rotation angle of the LC director varies continuously according to electrode position under an applied electric field, is proposed. Part of electrode is used for the *R*-region and the rest of part is used for the *T*-region. With optimized cell conditions, a single cell-gap and single gamma transflective LCD are achieved.

2. Cell structure and switching principle of the device

Fig. 1 shows a proposed cell structure of single cell-gap transflective associated with the FFS device. In a conventional FFS device, the common electrode is patterned with a plane shape and the pixel electrode is patterned with multiple numbers of slit, in which both electrodes are transparent. In the suggested transflective LCD, a part of plane shape of common electrode in *R*-region is composed for *R*-electrodes with embossing shape and it is electrically connected to the common electrode of *T*-region. The patterned ICR exists below the pixel electrodes with retardation of $\lambda/4$ only in the *R*-region and it is in isotropic state in the *T*-region.

* Corresponding authors. Tel.: +82 63 270 2343; fax: +82 63 270 2341 (S.H. Lee).
E-mail addresses: gdlee@dau.ac.kr (G.-D. Lee), lsh1@chonbuk.ac.kr (S.H. Lee).

1567-1739/$ - see front matter © 2010 Elsevier B.V. All rights reserved.
doi:10.1016/j.cap.2010.02.005

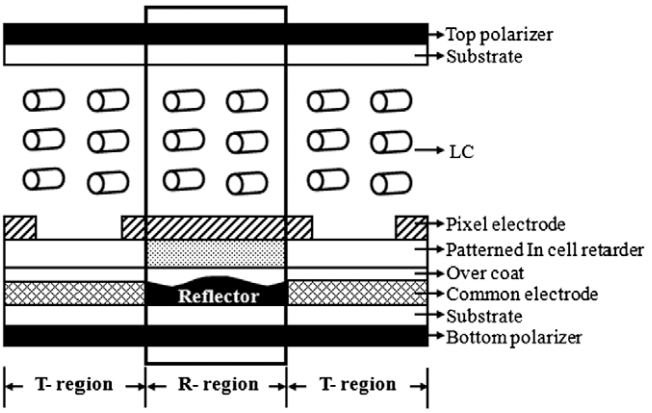

Fig. 1. Schematic cell structure of single cell-gap transflective display associated with the FFS device.

Here, the patterned in-cell retarder can be fabricated using a metal mask and UV in which details can be found from previous work [14,15]. The position of the ICR can be above pixel electrode too, depending upon the manufacturing process. The liquid crystals are homogeneously aligned and are rotated by a horizontal component of a fringe electric field. One interesting feature of the FFS device is that the twist angle of the LC in on state is strongly dependent on the electrode position due to different field intensity along the electrode position. Hence the twist angle is highest at the edge of pixel electrode and lowest at the center of pixel electrode [16].

In the device, uniaxial medium exists under crossed polarizer in *T*-region whereas for *R*-region, the light is reflected back from the top polarizer hence under uniaxial medium exists under linear polarizer in *R*-region. The normalized T/T_o and reflectance (R/R_o) can be expressed as

$$\begin{aligned} T/T_o &= \sin^2 2\psi(V)\sin^2(\pi d\Delta n_{\text{eff}}(V,\theta,\phi)/\lambda) \\ R/R_o &= \sin^2 4\psi(V)\sin^2(\pi d\Delta n_{\text{eff}}(V,\theta,\phi)/\lambda) \end{aligned} \quad (1)$$

where ψ is an voltage-dependent angle between the input polarizer and LC director, d is a cell-gap, Δn_{eff} is the voltage and viewing angle dependent effective birefringence of the LC medium, and λ is the wavelength of incident light. According to Eq. (1), when a rubbing angle on the bottom substrate is coincident with one of the transmission axis of the crossed polarizers, the device appears to be black at normal direction. When LC directors in *R*- and *T*-regions rotates about 22.5° and 45° respectively, the device has the maximum light efficiency.

Fig. 2 shows an optical cell configuration of the proposed single cell-gap transflective LCD. In the initial state, the transmission axis of top polarizer and the optic axis of LC layer are coinciding with each other in all of the *R*- and *T*-regions. In the *R*-region, the optic axis of the ICR with $\lambda/4$ retardation makes 45° with respect to the top polarizer and reflector exists in bottom. In the *T*-region, the transmission axis of bottom polarizer exist perpendicular to the top polarizer.

In order to understand a polarization path change of proposed single cell-gap transflective LCD, we used Poincare sphere representation, as shown in Fig. 3. In the *R*-region, in the absence of an electric field, the linearly polarized light (P1) comes out from the polarizer propagates along the slow axis of the LC director without changing its polarization state and after passing through the ICR, the light becomes circularly polarized light (P2) and after reflection, the circularly polarized light propagates through the ICR again and hence gain converts to the linearly polarized with a phase change of 90° (P3) from the original incident light, as shown in Fig. 3a. As a result, the light cannot pass through the analyzer and thus the *R*-region appears black. In the bright state, the LC directors rotates 22.5° due to fringe-field and the linearly polarized light changes to a 45° (P4) direction after passing through the liquid crystal. The linearly polarized light after passing through LC, proceed to ICR, which is also located at the optics axis of 45° with respect to the analyzer, hence the light goes without changing its polarization state. After reflection, the light again passing through ICR and goes through LC and hence linearly polarized after light

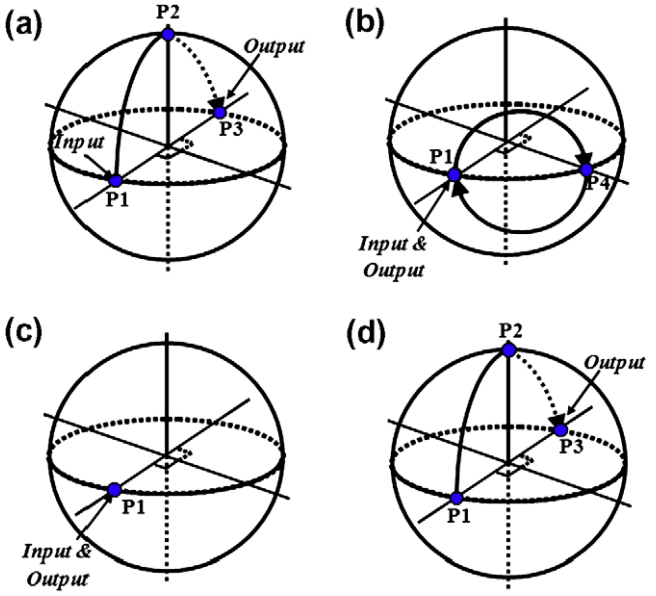

Fig. 3. Poincare sphere representation of the polarization path of the (a) dark and (b) white states in *R*-region and the (c) dark and (d) white states in *T*-region.

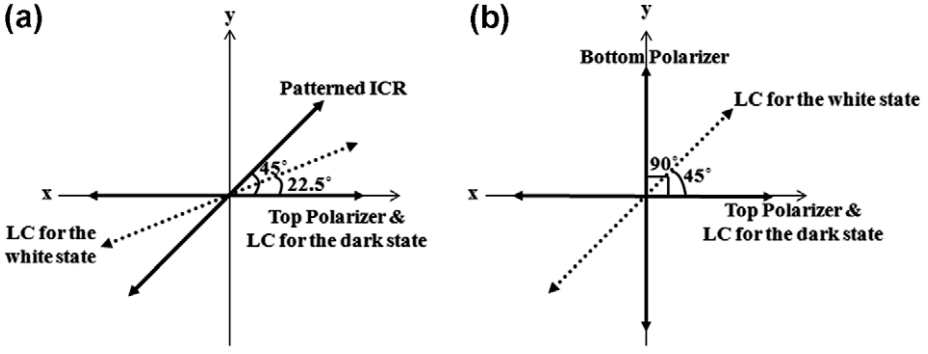

Fig. 2. Optical cell configuration in the (a) *R*- and (b) *T*-regions.

passing through LC comes back to its original polarization states of 0° (P1), resulting in a bright state, as shown in Fig. 3b. In the dark state of *T*-region, the linearly polarized light (P1) from the polarizer passes through LC layer without changing its polarization state. Thus it is blocked by the analyzer, showing a black state as shown in Fig. 3c. In the bright state, the LC director rotates 45° so that the input light (P1) is rotated 90° (P3), as shown in Fig. 3d. With above light path, the device is realized for normally black mode in both *R*- and *T*-regions. In the presence of an electric field, if the *R*-region is designed for an average twist angle of nearly $\psi = 22.5°$, and the *T*-region is designed for an average twist angle of nearly $\psi = 45°$, with $d\Delta n_{\text{eff}} = \lambda/2$ for both regions, maximal R/R_o and T/T_o can be achieved since it can rotate the linearly polarized light by 45° and 90°, in the *R*- and *T*-region, respectively.

3. Simulation conditions

In order to obtain single cell-gap and single gamma transflective FFS-LCD, a computer simulation was performed using the commercially available software, LCD master (Shintech, Japan) of which the optical calculation is based on 2×2 extended Jones Matrix [17]. For the simulation, dielectric anisotropy of the LC is 20 and the cell retardation is 0.40 μm with a cell-gap of 4 μm. The surface tilt angle of the LC is 2° with an initial rubbing direction of 80° with respect to its horizontal field. The T/T_o of the single polarizer and double polarizer with same transmission axis were assumed to be 41%, and 35%, respectively. To achieve a proper twist angle in each region, the electrode width is varied from 6 μm to 12 μm while the distance between two slit electrodes is fixed to 3 μm. Here, thickness of the ICR is 1 μm with a dielectric constant of 5.

4. Results and discussion

Fig. 4 shows twist angle distribution of LC at three different positions according to the electrode width in the white state. In the FFS device, a fringe electric field composed of vertical and horizontal component is generated when a voltage is applied. As indicated, the twist angle of the LC strongly depends on the electrode

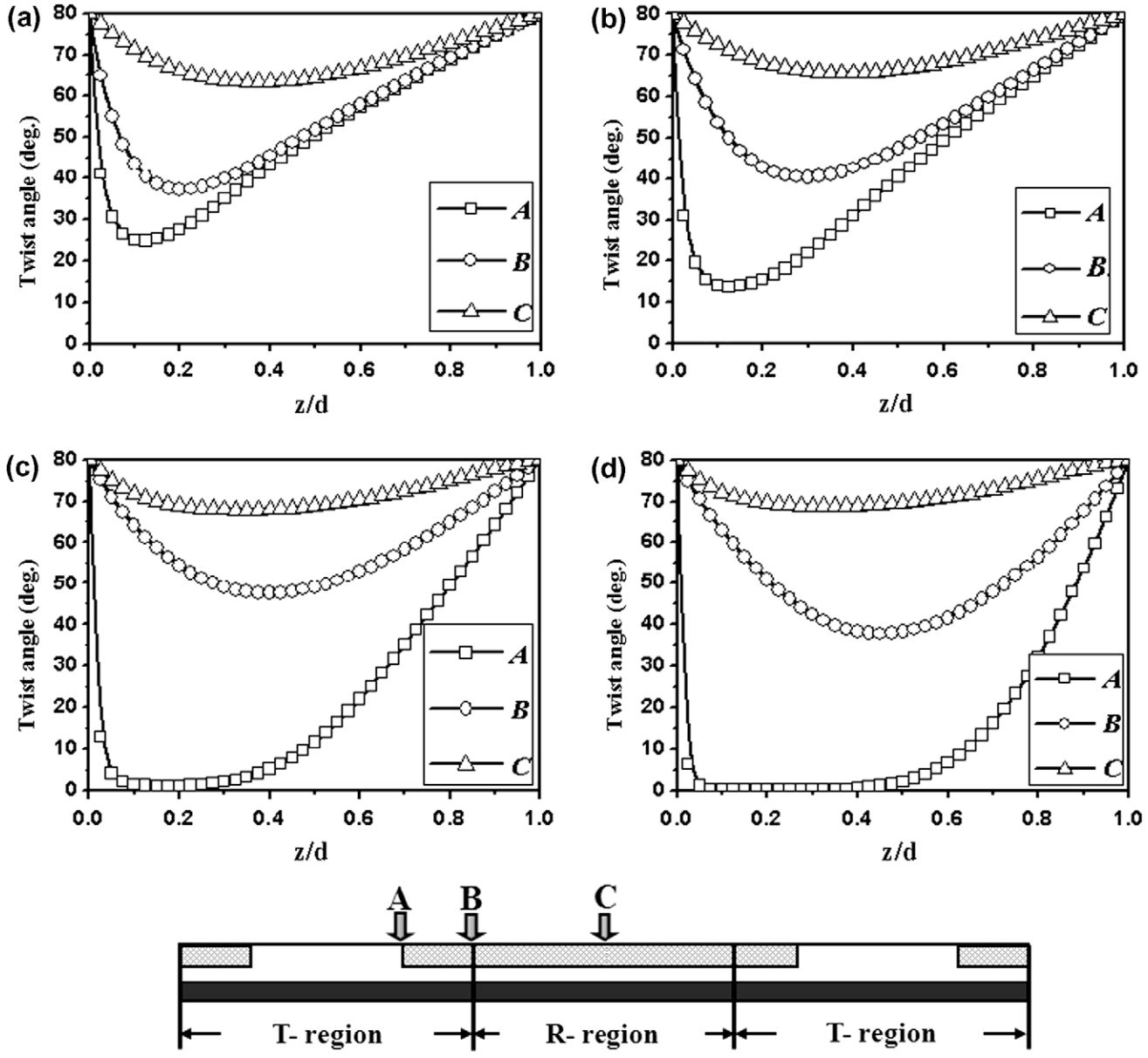

Fig. 4. Twist angle distribution of the LC at three different positions according to electrode width; (a) width = 6 μm, (b) width = 8 μm, (c) width = 10 μm, and (d) width = 12 μm.

position and width of pixel electrode. When the electrode width becomes 12 μm, the difference in twist angle between electrode positions of A B, and C is largest. In addition, the average twist angle at electrode positions B and C is found to be well below than 22.5° (see Fig. 4d) and hence not suitable to get the maximal R/R_o. The average twist angle of 22.5° is required to have maximal R/R_o. However, in other cases of 6 μm, 8 μm, and 10 μm electrode widths, the R/R_o was observed to be above than 30% (light efficiency is above 80%) with the *R*-regions.

To match gamma curve of the *R*- and *T*-regions, we calculated voltage-dependent R/R_o and T/T_o curves according to electrode width as shown in Fig. 5. From this, the operation voltage in *R*-region with electrode width of 6 μm is very low such as 5 V. On the other hand, in electrode width of 12 μm, the operation voltage in *R*-region is as high as 11 V. As a result, the operation voltage in *R*-region shows it is also significantly influenced by electrode width.

In case of electrode width of 6 μm, the operation voltage in *R*-regions is the lowest compared with other conditions, however it is not matched with operation voltage of *T*-region. Among four different electrode widths, the desired conditions of low operation voltage and a single gamma curve in both *R*- and *T*-region can be realized with an electrode width of 8 μm. Fig. 6 shows normalized voltage-dependent R/R_o and T/T_o curves with 8 μm electrode width. To achieve perfectly coincident voltage-dependent R/R_o and T/T_o curves, the curves are normalized by 95% of maximal T/T_o. In this case, the operating voltage in both regions is 6.5 V. In this device, not only do the operating voltage matches, but also the device can be driven by single gamma curve for both *R*- and *T*-regions. Therefore, a single cell-gap, and true single gamma transflective display using the FFS device can be achieved.

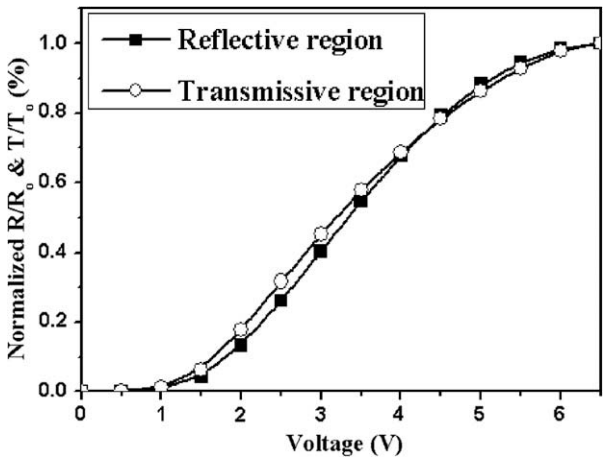

Fig. 6. Normalized voltage-dependent R/R_o and T/T_o curves with 8 μm electrode width.

Fig. 7 shows viewing angle characteristics of suggested transflective FFS display at the 550 nm. In the *R*-region, the region in

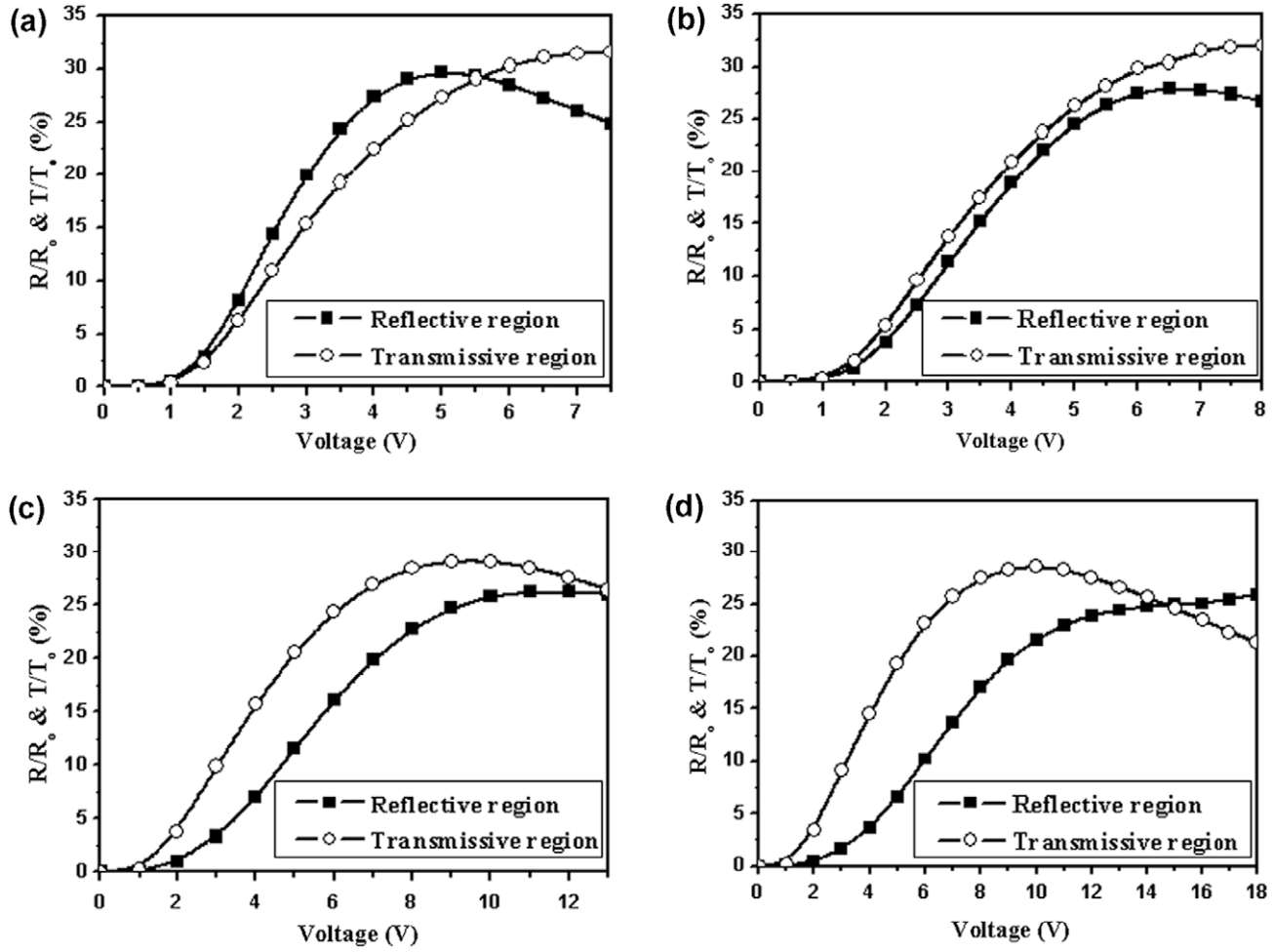

Fig. 5. Calculated voltage-dependent R/R_o and T/T_o according to electrode width; (a) width = 6 μm, (b) width = 8 μm, (c) width = 10 μm, and (d) width = 12 μm.

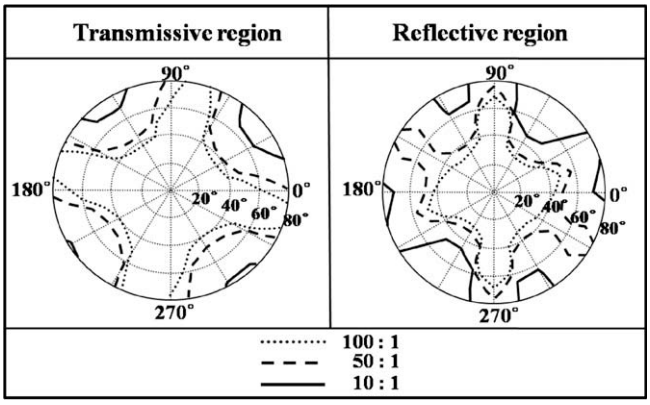

Fig. 7. Calculated iso-contrast ratio curves at a wavelength of 550 nm.

which the contrast ratio (CR) is large than 10 exist over 60° of the polar angle in all directions. Also, in the *T*-region, that region exists over 70° of the polar angle in all directions. Consequently, the device shows very wide viewing angle characteristics in both *T*- and *R*-regions.

5. Conclusions

A single cell-gap and single gamma transflective FFS-LCD with ICR was proposed. This device utilizes unique behavior of the FFS device such that the twist angle of the LC director strongly depends on the electrode position, which allows part of electrodes to be used for the R/R_o with high light efficiency. In addition, this device has advantages that it does not require additional compensation films, easy in manufacturing due to single cell-gap, and low cost due to single gamma characteristics with its excellent performances such as low power consumption, high light efficiency, and wide viewing angle.

Acknowledgements

This work was supported by the Korea Science and Engineering Foundation (KOSEF) grant funded by the Korea government (MOST) (No. R01-2007-000-20050-0) and WCU program through MEST (R31-2008-000-20029-0).

References

[1] H.-I. Baek, Y.-B. Kim, K.-S. Ha, D.-G. Kim, S.-B. Kwon, in: Proceeding of the 7th International Display Workshops, Society for Information Display, Hiroshima, Japan, 2002, p. 41.
[2] M. Jisaki, H. Yamaguchi, in: Proceeding of the 8th International Display Workshops, Society for Information Display, Nagoya, Japan, 2001, p. 133.
[3] C. Lo, T.-C. Yang, C.-J. Hu, C.-S. Cheng, C.-M. Chang, F.-Y. Gan, SID Int. Symp. Dig. Tech. Pap. 38 (2007) 714.
[4] G.-H. Kim, S.-H. Moon, J.-D. Noh, S.-C. Kim, W.S. Park, T.-H. Yoon, J.C. Kim, S.H. Hong, S.H. Lee, Jpn. J. Appl. Phys. 39 (2000) L221.
[5] J.H. Song, S.H. Lee, Jpn. J. Appl. Phys. 43 (2004) L1130.
[6] S.H. Lee, S.H. Hong, H.Y. Kim, G.-D. Lee, T.-H. Yoon, Jpn. J. Appl. Phys. 40 (2001) 5334.
[7] T.B. Jung, J.C. Kim, S.H. Lee, Jpn. J. Appl. Phys. 42 (2003) L464.
[8] J.H. Song, Y.J. Lim, M.-H. Lee, S.H. Lee, S.T. Shin, Appl. Phys. Lett. 87 (2005) 11108.
[9] O. Itou, S. Hirota, J. Tanno, M. Morimoto, K. Igeta, H. Imayama, S. Komura, T. Nagata, in: Proceeding of the 13th International Display Workshops, Society for Information Display, Otsu, Japan, 2006, p. 635.
[10] Y.J. Lim, M.-H. Lee, G.-D. Lee, W.-G. Jang, S.H. Lee, J. Phys. D: Appl. Phys. 40 (2007) 2759.
[11] S. Hirota, S. Oka, O. Itou, K. Igeta, M. Morimoto, H. Imayama, S. Komura, T. Nagata, SID Int. Symp. Dig. Tech. Pap. 38 (2007) 1661.
[12] N. Koma, M. Mitsu, Y. Tanaka, K. Endo, SID Int. Symp. Dig. Tech. Pap. 38 (2007) 1270.
[13] Y.H. Jeong, Y.J. Lim, E. Jeong, W.G. Jang, S.H. Lee, Liq. Cryst. 35 (2008) 187.
[14] D.J. Broer, J. Lub, G.N. Mol, Macromolecules 26 (1993) 1244.
[15] J. Kim, Y.-W. Lim, S.-D. Lee, Jpn. J. Appl. Phys. 45 (2006) 810.
[16] I.H. Yu, I.S. Song, J.Y. Lee, S.H. Lee, J. Phys. D: Appl. Phys. 39 (2006) 2367.
[17] A. Lien, Appl. Phys. Lett. 57 (1990) 2767.